

Power Spectrum of Primordial Inhomogeneity Determined from the 4-Year *COBE*¹ DMR Sky Maps

K.M. Górski^{2,3,4}, A.J. Banday^{2,5}, C.L. Bennett⁶, G. Hinshaw², A. Kogut², G.F. Smoot⁷,
and E.L. Wright⁸

ABSTRACT

Fourier analysis and power spectrum estimation of the cosmic microwave background anisotropy on an incompletely sampled sky developed by Górski (1994) has been applied to the high-latitude portion of the 4-year *COBE* DMR 31.5, 53 and 90 GHz sky maps. Likelihood analysis using newly constructed Galaxy cuts (extended beyond $|b| = 20$ deg to excise the known foreground emission) and simultaneously correcting for the faint high latitude galactic foreground emission is conducted on the DMR sky maps pixelized in both ecliptic and galactic coordinates. The Bayesian power spectrum estimation from the foreground corrected 4-year *COBE* DMR data renders $n \sim 1.2 \pm 0.3$, and $Q_{rms-PS} \sim 15.3_{-2.8}^{+3.7}$ μK (projections of the two-parameter likelihood). These results are consistent with the Harrison-Zel'dovich $n = 1$ model of amplitude $Q_{rms-PS} \sim 18$ μK detected with significance exceeding 14σ ($\delta Q/Q \lesssim 0.07$). (A small power spectrum amplitude drop below the published 2-year results is predominantly due to the application of the new, extended Galaxy cuts.)

Subject headings: cosmic microwave background — cosmology: observations — methods: analytical, statistical — large scale structure of the universe

¹The National Aeronautics and Space Administration/Goddard Space Flight Center (NASA/GSFC) is responsible for the design, development, and operation of the *Cosmic Background Explorer (COBE)*. Scientific guidance is provided by the *COBE* Science Working Group. GSFC is also responsible for the analysis software and for the production of the mission data sets.

²Hughes/STX Corporation, LASP, Code 685, NASA/GSFC, Greenbelt, Maryland 20771.

³on leave from Warsaw University Observatory, Aleje Ujazdowskie 4, 00-478 Warszawa, Poland.

⁴e-mail: gorski@stars.gsfc.nasa.gov

⁵Max Plank Institut fur Astrophysik, 85740 Garching Bei Munchen, Germany.

⁶Laboratory for Astronomy and Solar Physics, Code 685, NASA/GSFC, Greenbelt, Maryland 20771.

⁷LBL, SSL, & CfPA, Bldg 50-351, University of California, Berkeley CA 94720.

⁸UCLA Astronomy Department, Los Angeles CA 90024-1562.

1. INTRODUCTION

Following the seminal *COBE* DMR discovery of the anisotropy of the cosmic microwave background (CMB) after one year (1989/90) of observations (Smoot *et al.* 1992, Bennett *et al.* 1992, Wright *et al.* 1992, Kogut *et al.* 1992) the instrument continued operating until late 1993. Intermediate, 2-year results of the mission were reported by Bennett *et al.* (1994) (also see e.g. Górski *et al.* 1994, Wright *et al.* 1994). An overview of the 4-year results is provided by Bennett *et al.* (1996). In this paper we apply the CMB anisotropy power spectrum estimation technique introduced by Górski (1994) to the definitive, 4-year 31.5, 53, and 90 GHz sky maps resulting from the *COBE* DMR mission.

The *COBE* DMR-detected anisotropy of the CMB provides a unique opportunity to measure the spatial distribution of the inhomogeneities in the universe on the comoving scales ranging from a few hundred Mpc up to the present horizon size (inaccessible to any other astronomical observations) during the embryonic stage of their evolution, thereby avoiding the complications of (cosmologically) recent evolution of most astrophysical systems. There are, however, important experimental/observational limitations on the extent to which cosmologically interesting quantities can be extracted from the DMR data. These are imposed by our understanding of systematic effects, instrumental noise properties, and non-cosmological foreground signals peculiar to our location in the Galaxy and in the universe, and were investigated as follows. Kogut *et al.* (1996c) have addressed systematic effects in considerable detail and found them to be unimportant relative to the accuracy to which cosmological parameters can be determined from the DMR 4-year data. Górski *et al.* (1996) provide a comprehensive description of the noise properties of the DMR sky maps and demonstrate the sufficiency of the DMR noise models (see also Lineweaver *et al.* 1994). Emission from the galactic plane cannot yet be modelled to adequate precision and must be excised from the data (see §2 and Banday *et al.* 1996a). Foreground galactic emission at high latitude (Bennett *et al.* 1992, Kogut *et al.* 1996a,b) can be partially accounted for by using Galaxy-dominated spatial templates at frequencies where the CMB does not dominate (see §3, and Kogut *et al.* 1996a,b). The potential contamination of the CMB anisotropy by the astrophysical foregrounds outside of our Galaxy is demonstrated to be negligible in Banday *et al.* (1996b).

In this work we focus on a general characterization of the 4-year DMR sky maps in terms of a power spectrum of the angular distribution of the CMB temperature fluctuations and attempt to estimate its sensitivity to a plausible foreground emission contamination. We follow and further develop the method introduced by Górski (1994, hereafter G94a) and applied to the 2-year DMR data in Górski *et al.* (1994, hereafter G94b). As a useful power spectrum parametrization, we utilize a power-law family specified by Q_{rms-PS} and n — the amplitude and shape parameters (Bond & Efstathiou 1987, Fabbri, Lucchin, & Matarrese 1987), but we abbreviate the symbol Q_{rms-PS} and use Q instead. The results of the analysis involving the CMB spectra of specific large scale structure models will be presented elsewhere. Hereafter, bold letters denote matrices (upper case) and vectors (lower case), and p is a pixel label.

2. DATA

Our published analysis of the 2-year DMR data (G94b) involved a simple $|b| > 20^\circ$ Galaxy cut, which retained the relatively bright foreground emission from the Scorpius-Ophiucus and Taurus-Orion regions (de Vaucouleurs 1955). In this work we employ new, extended galactic cuts (see Banday *et al.* 1996a) which further excise these regions from the data used for the inference of the cosmological CMB anisotropy. We consider both extended $|b| > 20^\circ$ (denoted ‘20+’) and extended $|b| > 30^\circ$ (‘30+’) Galaxy cuts. We analyze the DMR sky maps in both ecliptic (‘E’) and galactic (‘G’) pixelization. To facilitate a comparison of the 4-year results with the published analyses of the 2-year data we re-apply the simple $|b| > 20^\circ$ Galaxy cut. From a total of 6144 data pixels on the entire sky, the following numbers of pixels remain for analysis after applying the different galactic cuts: 4038 for E20, 4016 for G20, 3890 for E20+, 3881 for G20+, 3039 for E30+, and 3056 for G30+.

We form weighted average maps at each frequency by combining the A and B channels,

$$\begin{aligned}\Delta_{31} &= 0.611 \Delta_{31A} + 0.389 \Delta_{31B}, \\ \Delta_{53} &= 0.579 \Delta_{53A} + 0.421 \Delta_{53B}, \\ \Delta_{90} &= 0.382 \Delta_{90A} + 0.618 \Delta_{90B},\end{aligned}\tag{1}$$

minimizing the cut-sky-averaged noise variance per pixel in the combined maps. The weighted 31.5, 53, and 90 GHz 4-year cut-sky DMR maps are analyzed jointly (equivalent to coaddition) with and without the foreground correction, or linearly combined (after foreground correction, indicated by tilde) with the weights designed to remove any leftover free-free emission:

$$\tilde{\Delta}_{CMB} = -0.302 \tilde{\Delta}_{31} + 0.633 \tilde{\Delta}_{53} + 0.669 \tilde{\Delta}_{90}.\tag{2}$$

The weights given to both 31.5 and 90 GHz maps in this linear combination technique are considerably larger than those in the coadded technique (~ 0.08 and ~ 0.26 , respectively). As a result, the noise is larger in the linear combination map $\tilde{\Delta}_{CMB}$, slightly exceeding the rms noise in the 90 GHz map alone.

Fourier analysis of the cut-sky maps is performed (see G94a for details) in the 961-dimensional linear space spanned by the orthonormal functions $\boldsymbol{\psi}$, which are linear combinations of spherical harmonics with $\ell \leq 30$. A sky map at frequency ν , $\Delta_\nu(p)$ (where p is the pixel label) is Fourier decomposed as follows

$$c_{i,\nu} = \frac{4\pi}{6144} \sum_{p \in \{cut\ sky\}} \Delta_\nu(p) \psi_i(p) \quad \text{and} \quad \Delta_\nu(p)|_{p \in \{cut\ sky\}} = \mathbf{c}_\nu^T \cdot \boldsymbol{\psi}(p).\tag{3}$$

Fourier coefficients c_i are linear in pixel temperatures, and account for the cut-sky mode coupling explicitly. Figure 1 (Color plate) displays an example of the $\boldsymbol{\psi}$ basis function constructed for various versions of the Galaxy cut used in this work.

The dominant component (in rms per pixel) of the raw, dipole-subtracted, cut-sky DMR maps is the instrument generated noise. A correct statistical modeling of this contaminant is essential for any method attempting to quantify the cosmological CMB anisotropy. A detailed analysis of noise properties of the entire DMR data set is discussed in Górski *et al.* (1996). Here we employ the noise modeling in Fourier space as described in G94a,b. The noise content of the 4-year DMR data is characterized by the rms noise amplitudes per Fourier mode of approximately 10.5, 3.4, and 5.5 μK at 31.5, 53, and 90 GHz, respectively. The coaddition of all available measurements at three frequencies renders a map with the rms noise amplitude per Fourier mode of $\sim 2.7 \mu\text{K}$.

3. LIKELIHOOD ANALYSIS OF FOREGROUND CORRECTED DMR SKY MAPS

Following G94a,b, we conduct Bayesian inference from the *COBE* DMR data of the power spectrum of primordial CMB anisotropy under the usual assumption that the measurement (here the joint vector of coefficients of Fourier decomposition of the 31.5, 53, and 90 GHz sky maps, $\hat{\mathbf{c}}_{\Psi}^T \equiv (\hat{\mathbf{c}}_{31.5}^T, \hat{\mathbf{c}}_{53}^T, \hat{\mathbf{c}}_{90}^T)$) is a sum of a signal — primordial CMB anisotropy, and noise — a random, receiver generated contamination, and that both these components are Gaussian stochastic variables. Hence, the likelihood function is *exactly* represented as a multivariate Gaussian in variable \mathbf{c}_{Ψ} . The likelihood density is fully specified by the Fourier space correlation matrices of signal, \mathbf{C}_S , a function of the assumed (and tested) power spectrum of the CMB anisotropy, and noise (at a given frequency ν), $\mathbf{C}_{N_{\nu}}$, which are computed as described in G94a,b. No approximations or Monte Carlo simulations are required for evaluation of the likelihood function, and this power spectrum parameter estimation technique, bi-linear in the measurement values of temperature perturbations, is statistically unbiased.

This formulation of the likelihood problem allows one naturally to address a problem of contamination of the CMB anisotropy data by the diffuse foreground emission. Assume (generally) that the anisotropy, \mathbf{c}_{ν} , is measured at M frequencies ν , and the foreground emission can be measured or modeled as a certain number, N , of non-stochastic spatial templates $F_k(p)$ (whose Fourier transforms are \mathbf{f}_k , $k = 1, \dots, N$). The template corrected joint data vector, $\tilde{\mathbf{c}}_{\Psi}$, and its covariance matrix, $\mathbf{C}_{SN_{\Psi}}$, are

$$\tilde{\mathbf{c}}_{\Psi} = \begin{pmatrix} \hat{\mathbf{c}}_{\nu_1} - \sum_{k=1}^{k=N} \alpha_{\nu_1}^k \mathbf{f}_k \\ \dots \\ \hat{\mathbf{c}}_{\nu_M} - \sum_{k=1}^{k=N} \alpha_{\nu_M}^k \mathbf{f}_k \end{pmatrix}, \quad \mathbf{C}_{SN_{\Psi}} = \langle \tilde{\mathbf{c}}_{\Psi} \cdot \tilde{\mathbf{c}}_{\Psi}^T \rangle = \begin{pmatrix} \mathbf{C}_{SN_{\nu_1}} & \dots & \mathbf{C}_S \\ \dots & \dots & \dots \\ \mathbf{C}_S & \dots & \mathbf{C}_{SN_{\nu_M}} \end{pmatrix}, \quad (4)$$

where the matrix $\mathbf{C}_{SN_{\nu_i}} = \mathbf{C}_S + \mathbf{C}_{N_{\nu_i}}$ specifies the Gaussian probability distribution of the receiver noise contaminated theoretical CMB anisotropy signal at a given frequency ν_i . With these definitions the likelihood function takes the usual form

$$P(\tilde{\mathbf{c}}_{\Psi}) \propto \exp\left(-\tilde{\mathbf{c}}_{\Psi}^T \cdot \mathbf{C}_{SN_{\Psi}}^{-1} \cdot \tilde{\mathbf{c}}_{\Psi} / 2\right) / \sqrt{\det \mathbf{C}_{SN_{\Psi}}}. \quad (5)$$

This is a function of all parameters used to describe the CMB power spectrum and $M \times N$ coefficients α_ν^i used in the foreground correction. For a given CMB power spectrum (i.e. a fixed \mathbf{C}_S) the likelihood can be maximized with respect to parameters α_ν^i , as a usual χ^2 fitting problem (naturally, the dimensionality of the data vector is presumed to be large compared to both M and N). From the maximum likelihood equations, $\partial \ln P / \partial \alpha_\nu^i = 0$, one derives the following set of linear equations (for a given ν and k):

$$\sum_{j, \nu'} \mathbf{f}_k^T \cdot (\mathbf{C}_{SN\oplus}^{-1})_{\nu\nu'} \cdot \mathbf{f}_j \alpha_{\nu'}^j = \sum_{\nu''} \mathbf{f}_k^T \cdot (\mathbf{C}_{SN\oplus}^{-1})_{\nu\nu''} \cdot \hat{\mathbf{c}}_{\nu''}, \quad (6)$$

which render the maximum likelihood solutions $\hat{\alpha}_\nu^k$. The parameter covariance matrix (dimension $(M \times N)^2$) is

$$M_{\alpha\alpha'}^{-1} \equiv -\frac{\partial^2 \ln P}{\partial \alpha_\nu^k \partial \alpha_{\nu'}^{k'}} = \mathbf{f}_k^T \cdot (\mathbf{C}_{SN\oplus}^{-1})_{\nu\nu'} \cdot \mathbf{f}_{k'}. \quad (7)$$

In both equations $(\mathbf{C}_{SN\oplus}^{-1})_{\nu\nu'}$ is a square portion of the inverse covariance matrix $\mathbf{C}_{SN\oplus}^{-1}$ acting between frequencies ν , and ν' .

We apply this formalism to study the sensitivity of parametrization of the cosmological anisotropy derived from the DMR data to the possible contamination by high latitude galactic foreground emission. We assume that the faint foreground glow of synchrotron, free-free, and dust emission outside the galactic plane can be traced by the available templates from observations at frequencies where the CMB does not dominate. Two plausible selections (Kogut *et al.* 1996a,b) are the *DIRBE* 140 μm data (Reach *et al.* 1995), and the 408 MHz full sky radio map (Haslam *et al.* 1980). (We also used the 110, and 240 μm *DIRBE* data and found the coupling of these to the DMR frequencies indistinguishable from that derived at 140 μm .) We conduct the analysis as outlined above with $M = 3$ DMR frequencies and $N = 2$ templates. Together with the CMB parameters Q and n this constitutes an 8-dimensional likelihood problem. (A further extension of the method, described in Banday *et al.* 1996b, addresses the issue of cross-correlation of the DMR data with existing catalogues of extragalactic objects; there we have employed $N = 6$ templates, and solved the 20-dimensional likelihood problem.) For each Galaxy cut selection we evaluate the Q - n likelihood both without and with the foreground correction applied to the data. At each Q - n grid point we derive the maximum likelihood solutions $\hat{\alpha}_\nu^i(Q, n)$ (and their covariance matrix), and use these values to evaluate the foreground corrected likelihood. Maximization of the corrected likelihood renders simultaneously the most likely solution of both the cosmological (Q - n), and foreground ($\hat{\alpha}_\nu^i$) fitting problem. The likelihood surface in Q and n is sharply peaked (as shown in G94b for 2-year data), and despite it being non-Gaussian in functional form, the average values of the foreground coupling constants ($\langle \hat{\alpha}_\nu^i(Q, n) \rangle$, weighted by the corrected likelihood) turn out practically identical to the maximum likelihood solutions. The likelihood averaged values of the six coupling constants between the three DMR maps and the 140 μm and 408 MHz data are shown in Fig. 2. The physical interpretation of these results in terms of the inferred contribution of galactic dust, free-free, and synchrotron emission in the high-latitude DMR sky maps is discussed

by Kogut *et al.* (1996a,b). Here, we proceed to discuss the primary target of the analysis of the foreground corrected DMR sky maps — the cosmic CMB anisotropy.

4. RESULTS

Fig. 3 (Color plate) shows the coadded, foreground corrected DMR sky maps in both the ecliptic and galactic coordinate pixelization. For visualization the maps have been “cleaned” by removing the $\ell > 40$ noise (the 7° FWHM DMR beam picks up sky signals that are entirely contained within $\ell \leq 40$ in Fourier space). Ecliptic and galactic maps appear very consistent at large angular scales, but near the pixel scale one can notice the localised effects of different noise binning depending on the reference frame. The choice of pixelization re-bins roughly half of the instrument noise while leaving the CMB anisotropy unchanged; consequently, slight variations in the likelihood results are expected.

Fig. 4 displays the cut sky DMR power spectra before and after the foreground correction evaluated for four combinations of pixelization and Galaxy cut. (These spectra are shown here for illustration purposes only; the likelihood method uses the Fourier coefficients c_i , not any quadratic function thereof.) The apparently steep power spectrum of the foreground Galaxy templates, $\sim \ell^{-3}$ at higher ℓ , was discussed by Kogut *et al.* (1996a). An important result of the simultaneous CMB background (Q, n) and foreground (α_ν^k) fitting is that the Galaxy correction affects only the very low order multipoles of the derived cosmic CMB anisotropy. Since the quadrupole moment of the Galaxy is partially counter-aligned to the CMB quadrupole (Kogut et al. 1996b), correcting the DMR maps for Galactic emission *increases* the estimated CMB quadrupole.

Table 1 provides a comprehensive summary of the maximum likelihood solutions for the CMB anisotropy power spectrum model parameters. The first entries in Table 1 refer to the high-latitude coadded DMR maps from which no model of Galactic emission has been removed and include, for comparison with the published 2-year analyses, the results of re-application of the $|b| = 20$ deg Galaxy cut. One should note the following: (1) compared to the G20 2-year results described in G94b, the 4-year DMR data render a slightly smaller, but statistically consistent, power spectrum normalization (roughly a $\sim 0.5 \mu\text{K}$ drop of $Q|_{n=1}$); (2) solutions for n are fairly stable with respect to variation of the Galaxy cut, but the derived anisotropy amplitude decreases by more than $1 \mu\text{K}$ upon removal of the bright Scorpius-Ophiucus and Taurus-Orion foreground regions (i.e. upon extension of Galaxy cut from ‘20’ to ‘20+’), (3) an extra, but smaller, decrease of the amplitude results from a further extension of Galaxy cut (to ‘30+’); we consider this as suggestive of having reached a sufficiently deep Galaxy plane excision with the ‘20+’ cut. Certainly the higher Galactic cut excludes real CMB features correlated over large areas of the sky in the range $20^\circ < |b| < 30^\circ$, which affects the $Q - n$ fits.

Comparing results for which the quadrupole is included ($\ell_{min} = 2$) to those from which it

has been excluded ($\ell_{min} = 3$), we find again a systematic shift to higher normalization and lower index n in the quadrupole-excluded results. The shift is well within the uncertainties from noise and cosmic variance, but reflects at least in part the counter-alignment of the CMB and Galactic quadrupoles: if the quadrupole is to be retained in the inference of cosmological parameters, Galactic emission should be accounted for in the data.

The next set of entries in Table 1 refers to the DMR maps corrected for Galactic emission using the 408 MHz survey to trace synchrotron emission and the DIRBE 140 μm map to trace dust emission. Free-free emission is removed using a linear combination of the dust- and synchrotron-corrected DMR maps. This map makes no assumptions as to the distribution of free-free emission, but is relatively noisy compared to the coadded maps, which is reflected in lower significance of all the derived parameters. The final set of entries refers to the maximally sensitive coadded maps, corrected for Galactic emission using the 408 MHz survey to trace synchrotron emission and the DIRBE 140 μm map to trace both dust and free-free emission. The fitted values for Q and n are in good agreement for both foreground correction techniques. One will note that the high latitude foreground correction further reduces the fitted power spectrum amplitude by $\sim 0.5 \mu\text{K}$. This cannot be considered as significant particularly in the light of a similar order of discrepancy between the galactic and ecliptic map maximum likelihood solutions, and especially in comparison with an overall statistical significance of all the determined parameters.

5. SUMMARY

A statistically unbiased technique of power spectrum determination has been used to infer the CMB normalization Q_{rms-PS} and power-law index n from the *COBE* DMR 4-year sky maps. The sky maps are decomposed in the basis of orthonormal functions on the cut sky into a set of coefficients linear in the pixel temperatures. These coefficients are then used in a likelihood analysis to infer the parameters of the CMB anisotropy models. We account for high-latitude Galactic emission by using the 408 MHz sky survey to trace the angular distribution of synchrotron emission and the DIRBE 140 μm map to trace dust emission. Free-free emission is removed using either a linear combination of the DMR maps or using the DIRBE map to remove free-free as well as dust emission. Since we find some minor changes in the fitted parameters with the Galaxy cut or map pixelization and method of high latitude foreground modeling, a judgement call is required to quote a unique *COBE* DMR determination of the primordial power spectrum parameters. The 4-year data are consistent with quadrupole normalization $Q_{rms-PS} \sim 15.3_{-2.8}^{+3.7} \mu\text{K}$ and power-law index $n \sim 1.2 \pm 0.3$. With n fixed at unity we derive the normalization for an exact scale-invariant Harrison-Zel'dovich power spectrum $Q_{rms-PS}|_{n=1} \sim 18 \mu\text{K}$ with high ($\gtrsim 14\sigma$) significance $\delta Q/Q \lesssim 0.07$. Implications of the *COBE* DMR 4-year data for the specific models of large scale structure formation will be discussed elsewhere.

We gratefully acknowledge the efforts of those contributing to the *COBE* DMR. *COBE* is supported by the Office of Space Sciences of NASA Headquarters.

REFERENCES

- Banday, A.J., et al. 1996a, ApJ (submitted)
- Banday, A.J., et al. 1996b, ApJ (submitted)
- Bennett, C.L., et al. 1992, ApJ, 396, L7
- Bennett, C.L., Banday, A.J., Górski, K. M., Hinshaw, G., Kogut, A., & Wright, E.L. 1996, ApJ (submitted)
- Bond, J. R., & Efstathiou, G. 1987, MNRAS, 226, 655
- de Vaucouleurs, G. 1956, *Vistas in Astronomy*, 2, 1584
- Fabbri, R., Lucchin, F., & Matarrese, S. 1987, ApJ, 315, 1
- Górski, K.M. 1994, ApJ, 430, L85 (G94a)
- Górski, K.M., et al. 1994, ApJ, 430, L89 (G94b)
- Górski, K.M., et al. 1996, ApJ (in preparation)
- Haslam, C.G.T, Klein, U., Salter, C.J., Stoffel, H, Wilson, W.E., Cleary, M.N., Cooke, D.J., & Thomasson, P. 1981, A&A, 100, 209
- Kogut, A., et al. 1992, ApJ, 401, 1
- Kogut, A., Banday, A.J., Bennett, C.L., Górski, K. M., Hinshaw, G., & Reach, W.T. 1996a, ApJ (in press)
- Kogut, A., Hinshaw, G., Banday, A.J., Bennett, C.L., Górski, K. M., & Smoot, G.F. 1996b, ApJ (submitted)
- Kogut, A., et al. 1996c, ApJ (submitted)
- Kogut, A., Banday, A.J., Bennett, C.L., Górski, K. M., & Hinshaw, G. 1996d, ApJ (submitted)
- Lineweaver, C., et al. 1994, ApJ, 436, 452
- Reach, W.T., Franz, B.A., Kelsall, T., & Weiland, J.L. 1995, *Unveiling the Cosmic Infrared Background*, ed. E. Dwek, (New York:AIP)
- Smoot, G. F. et al. 1992, ApJ, 396, L1
- Wright, E.L., et al. 1992, ApJ, 396, L13

FIGURE CAPTIONS

Fig. 1 (Color Plate). An example of the full-sky spherical harmonic and the related cut-sky orthonormal functions (Górski 1994) — note the coordinate frame and Galaxy cut dependence — used in Fourier analysis of the DMR and foreground emission template data.

Fig. 2. Coefficients of coupling between the three DMR channels at 31.5, 53, and 90 GHz and the Galactic templates: the $140\mu\text{m}$ *DIRBE* data — filled symbols, and the 408 MHz radio data — open symbols. The coefficients shown in the plot (computed for the choice of pixelization and Galaxy cut as indicated) are the maximum likelihood values averaged over the $(Q - n)$ likelihood of the simultaneous background and foreground fit to the 4-year DMR data. The one σ confidence intervals are defined in the usual manner as the square roots of the diagonal on the covariance matrix.

Fig. 3 (Color Plate). *COBE* DMR 4-year, 31.5, 53, and 90 GHz sky maps coadded after foreground correction according to the $140\mu\text{m}$ - and 408 MHz-template fitting. Galactic and ecliptic (rotated to galactic coordinates to facilitate the comparison) pixelizations are shown. Noise reducing Fourier removal of the $\ell > 40$ content of the raw data has been applied to the full sky maps in order to aid visualization. Apparent small differences in pixel temperatures are induced by the reference frame dependent time ordered data noise binning in the map making procedure.

Fig. 4. Power spectra of the coadded DMR data and the templates used to assess the galactic foreground emission. The four panels exhibit the cut-sky rms power spectra, $c_\ell \equiv \left[\left(\sum_{i=\ell^2+1}^{i=(\ell+1)^2} c_i^2 \right) / (2\ell + 1) \right]^{1/2}$, evaluated for both ecliptic and galactic data with two Galaxy cuts as indicated. (Small letter c_ℓ is used in the definition of the cut-sky spectrum to avoid confusion with commonly used C_ℓ symbols, which denote the theoreticall, full-sky anisotropy spectrum.) Open circles — coadded raw DMR data, filled circles — template corrected DMR data, filled squares — foreground emission contribution to the DMR 53 GHz data characterized by spatial structure of the $140\mu\text{m}$ *DIRBE* map, arrows — 95% upper limit to possible foreground emission in the DMR 53 GHz channel characterized by spatial structure of the 408 MHz radio data, horizontal lines — rms noise per Fourier mode in the coadded 4-year DMR maps.

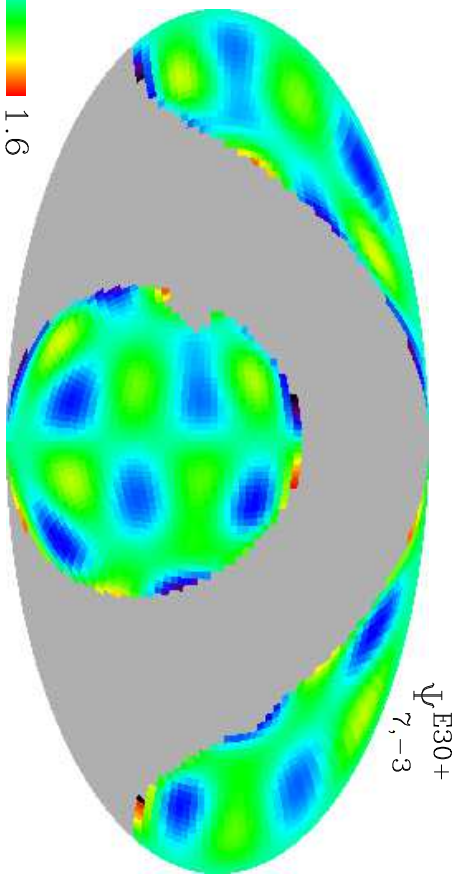
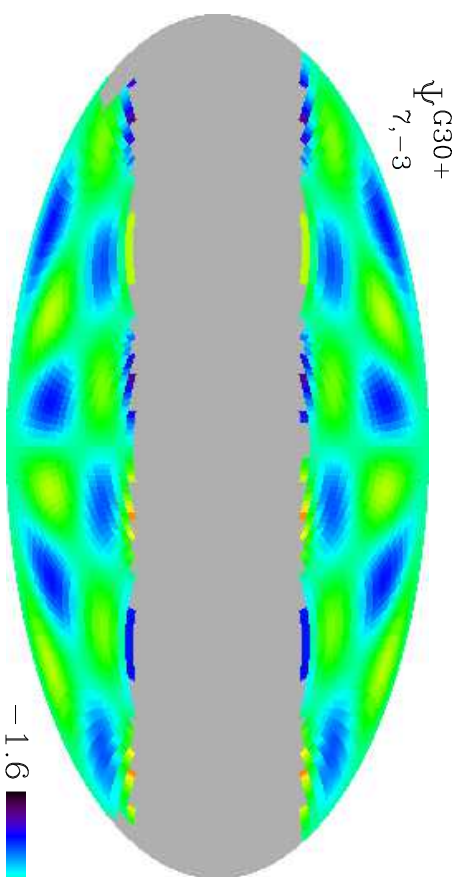
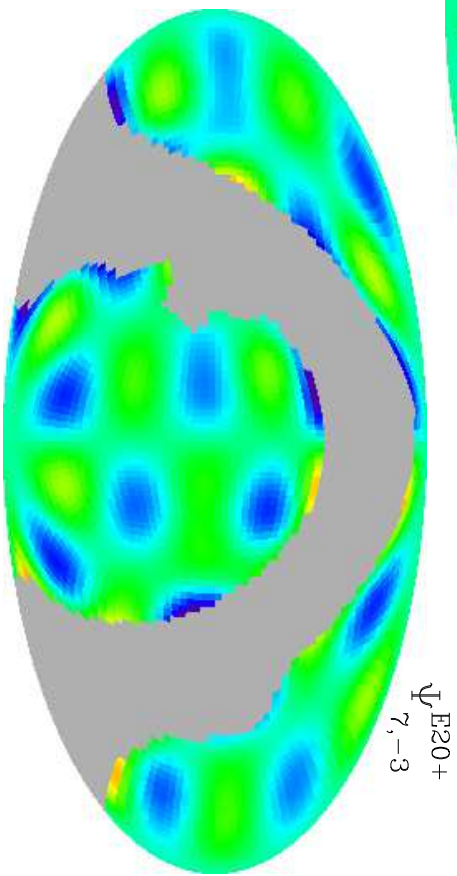
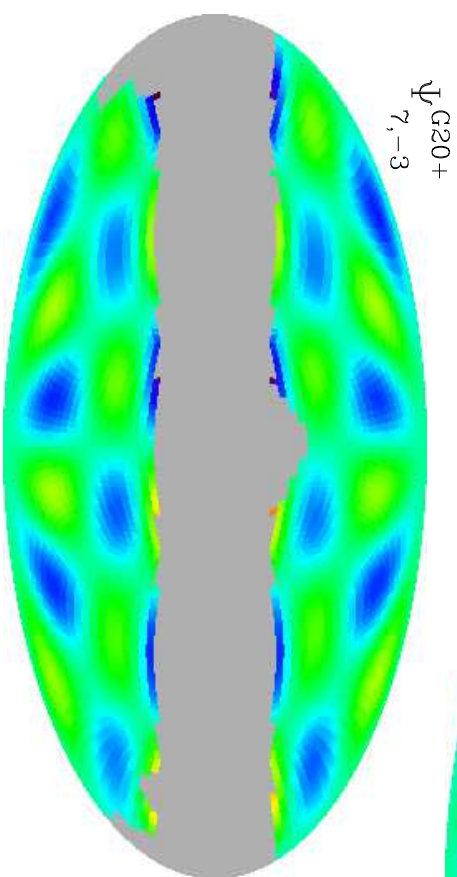
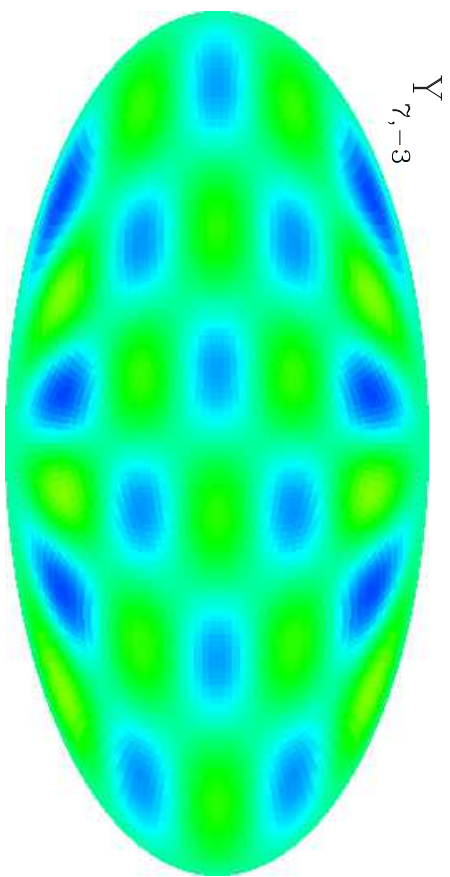
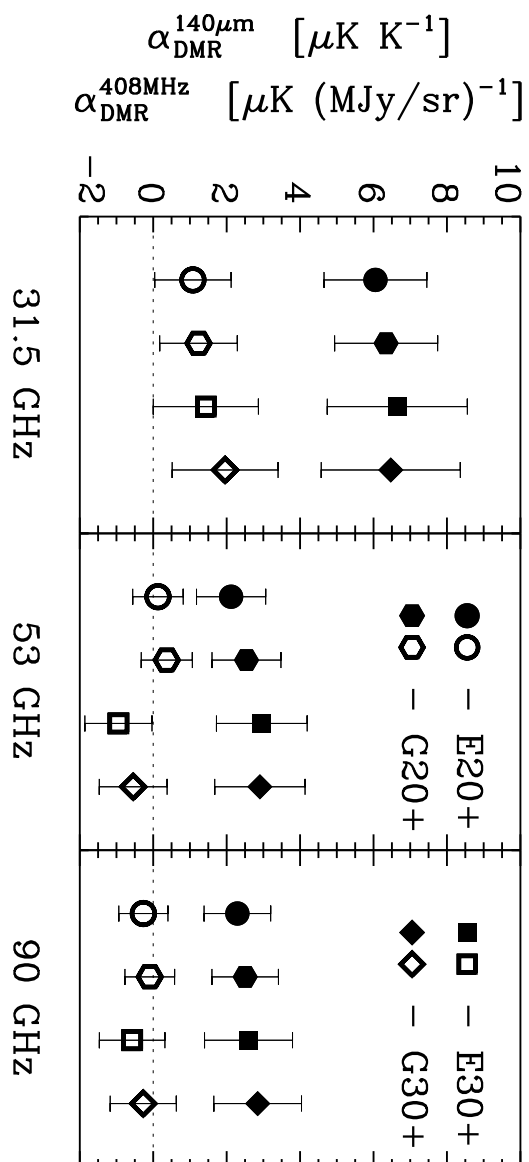


Table 1: Derived Parameters from the Likelihood Analysis of *COBE* DMR Four-Year Sky Maps^a

Reference Frame:		Ecliptic						Galactic																							
Galaxy Cut:		20		20+		30+		20		20+		30+																			
ℓ_{min}	parameter	Coadded Map: no galaxy correction																													
2	n	1.13	+0.26	+0.50	-0.27	-0.55	1.22	+0.24	+0.47	-0.28	-0.56	1.24	+0.30	+0.57	-0.29	-0.62	1.22	+0.24	+0.48	-0.28	-0.57	1.23	+0.23	+0.47	-0.29	-0.58	1.23	+0.29	+0.55	-0.34	-0.68
	Q_{rms-PS}	18.25	+4.46	+10.4	-3.31	-5.94	15.90	+3.93	+9.01	-2.73	-4.99	14.99	+3.93	+9.54	-3.02	-5.23	16.71	+3.93	+9.30	-3.12	-5.47	15.26	+3.93	+8.96	-2.64	-4.84	15.18	+4.46	+10.5	-2.92	-5.27
	$Q_{rms-PS} _{n=1}$	20.16	+1.34	+2.83	-1.25	-2.44	18.73	+1.25	+2.64	-1.20	-2.35	17.96	+1.44	+3.02	-1.34	-2.64	19.40	+1.29	+2.78	-1.25	-2.44	18.34	+1.25	+2.64	-1.20	-2.35	17.82	+1.44	+3.02	-1.34	-2.64
3	n	0.96	+0.28	+0.54	-0.30	-0.63	1.00	+0.28	+0.54	-0.29	-0.61	1.01	+0.32	+0.63	-0.35	-0.72	1.02	+0.28	+0.54	-0.29	-0.62	0.99	+0.28	+0.54	-0.30	-0.62	0.93	+0.34	+0.66	-0.36	-0.75
	Q_{rms-PS}	20.98	+6.04	+14.2	-4.12	-7.33	19.11	+5.08	+12.2	-3.84	-6.71	18.30	+5.80	+14.3	-4.17	-7.19	19.40	+5.23	+12.7	-4.03	-7.00	18.82	+4.89	+12.0	-3.88	-6.76	19.01	+6.38	+15.6	-4.41	-7.53
	$Q_{rms-PS} _{n=1}$	20.50	+1.34	+2.83	-1.29	-2.54	19.11	+1.25	+2.68	-1.25	-2.40	18.44	+1.49	+3.12	-1.39	-2.73	19.73	+1.34	+2.83	-1.25	-2.49	18.68	+1.29	+2.68	-1.20	-2.40	18.30	+1.49	+3.12	-1.39	-2.68
Linear Combination Map																															
2	n						1.29	+0.34	+0.69	-0.43	-0.87	1.19	+0.46	+0.88	-0.55	-1.14						1.11	+0.38	+0.73	-0.42	-0.87	0.79	+0.48	+0.92	-0.55	-1.07
	Q_{rms-PS}						15.75	+5.08	+12.3	-3.45	-6.09	15.80	+6.57	+16.3	-4.08	-7.05						16.33	+5.18	+12.8	-3.69	-6.38	18.63	+7.72	+18.8	-5.08	-8.58
	$Q_{rms-PS} _{n=1}$						18.58	+1.87	+3.88	-1.73	-3.40	17.53	+2.06	+4.36	-1.87	-3.64						17.38	+1.77	+3.74	-1.68	-3.74	16.57	+1.92	+4.08	-1.82	-3.50
Coadded Map: galaxy corrected																															
2	n						1.24	+0.23	+0.47	-0.29	-0.57	1.24	+0.29	+0.55	-0.29	-0.62						1.21	+0.24	+0.48	-0.28	-0.57	1.24	+0.27	+0.54	-0.33	-0.67
	Q_{rms-PS}						15.47	+3.55	+8.39	-2.78	-4.94	14.80	+3.79	+9.06	-2.88	-5.03						15.23	+3.69	+8.58	-2.64	-4.75	14.80	+4.07	+9.64	-2.83	-5.08
	$Q_{rms-PS} _{n=1}$						18.20	+1.25	+2.59	-1.20	-2.35	17.48	+1.44	+3.02	-1.34	-2.59						17.67	+1.25	+2.59	-1.15	-2.30	17.34	+1.39	+2.97	-1.34	-2.59

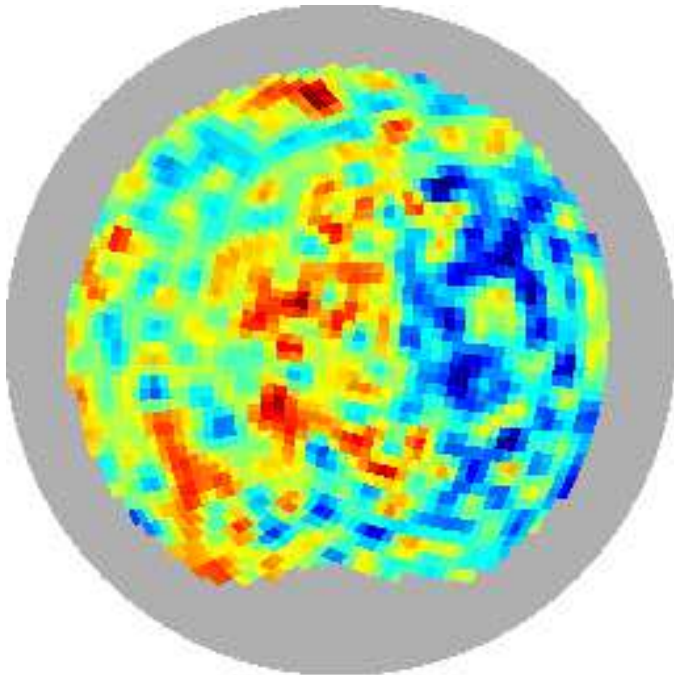
^aWe derive the tabulated values for Q and n by projecting the 2-dimensional, $Q - n$ likelihood function onto the Q or n axis (rather than marginalising) and quote the maximal likelihood value and the 68% and 95% credible intervals of the resulting 1-dimensional likelihood densities. We also evaluate the likelihood along the slice $n = 1$ to derive the CMB normalization for an exact Harrison-Zel'dovich power spectrum.



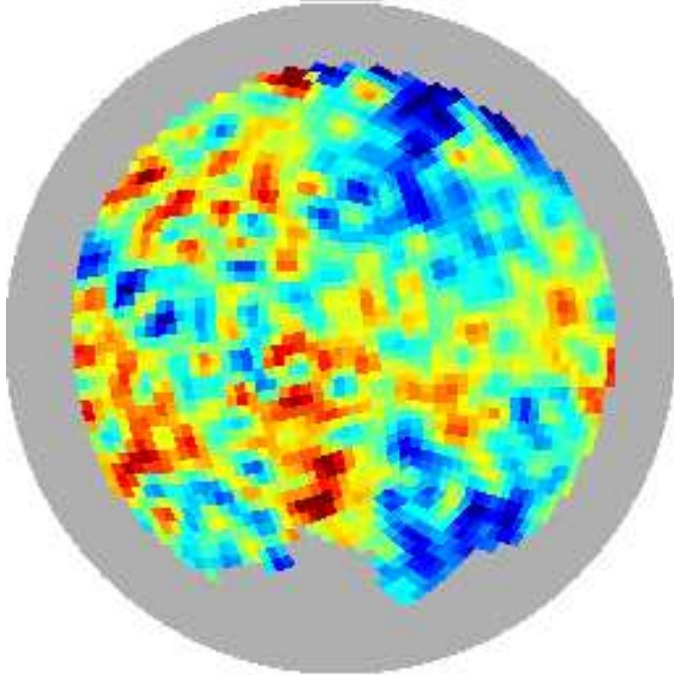
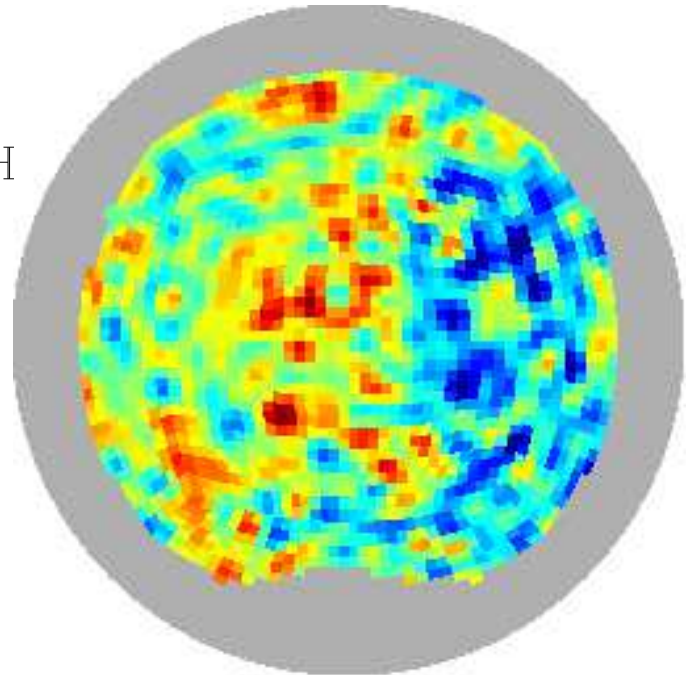
COBE-DMR Four-Year Sky Maps

Ecliptic Pixelisation

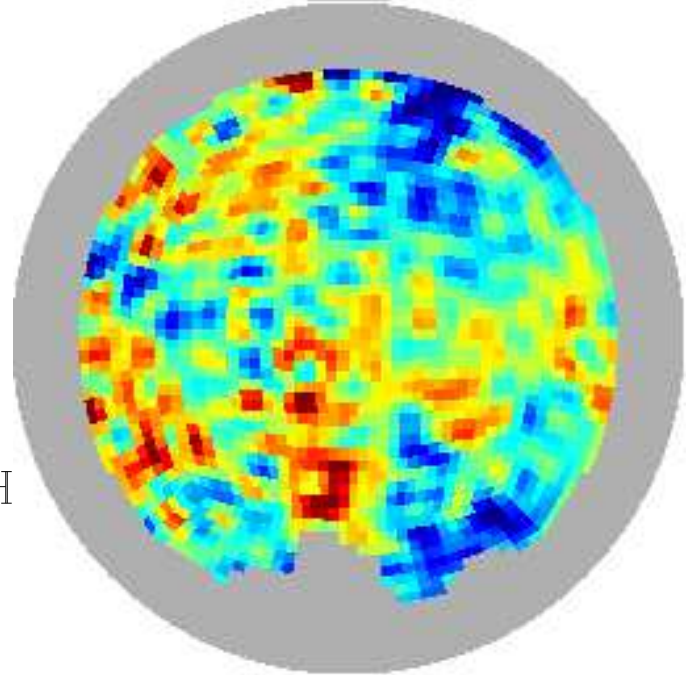
Galactic Pixelisation



NGH



SGH



$-130 \mu\text{K}$  $130 \mu\text{K}$

